

Individual Content and Motion Dynamics Preserved Pruning for Video Diffusion Models

Yiming Wu

The University of Hong Kong
Hong Kong, China

Zhenghao Chen*

University of Newcastle
Newcastle, Australia

Huan Wang

Westlake University
Hangzhou, China

Dong Xu*

The University of Hong Kong
Hong Kong, China

ABSTRACT

The high computational cost and slow inference time are major obstacles to deploying Video Diffusion Models (VDMs). To overcome this, we introduce a new Video Diffusion Model Compression approach using individual content and motion dynamics preserved pruning and consistency loss. First, we empirically observe that deeper VDM layers are crucial for maintaining the quality of **motion dynamics** (e.g., coherence of the entire video), while shallower layers are more focused on **individual content** (e.g., individual frames). Therefore, we prune redundant blocks from the shallower layers while preserving more of the deeper layers, resulting in a lightweight VDM variant called VDMini. Moreover, we propose an **Individual Content and Motion Dynamics (ICMD)** Consistency Loss to gain comparable generation performance as larger VDM to VDMini. In particular, we first use the Individual Content Distillation (ICD) Loss to preserve the consistency in the features of each generated frame between the teacher and student models. Next, we introduce a Multi-frame Content Adversarial (MCA) Loss to enhance the motion dynamics across the generated video as a whole. This method significantly accelerates inference time while maintaining high-quality video generation. Extensive experiments demonstrate the effectiveness of our VDMini on two important video generation tasks, Text-to-Video (T2V) and Image-to-Video (I2V), where we respectively achieve an average $2.5 \times$, $1.4 \times$, and $1.25 \times$ speed up for the I2V method SF-V, the T2V method T2V-Turbo-v2, and the T2V method HunyuanVideo, while maintaining the quality of the generated videos on several benchmarks including UCF101, VBench-T2V, and VBench-I2V.

CCS CONCEPTS

• Information systems → Multimedia content creation.

KEYWORDS

Video Generation, Model Compression, Distillation

ACM Reference Format:

Yiming Wu, Zhenghao Chen*, Huan Wang, and Dong Xu*. 2025. Individual Content and Motion Dynamics Preserved Pruning for Video Diffusion Models. In *Proceedings of the 33rd ACM International Conference on Multimedia*

Permission to make digital or hard copies of all or part of this work for personal or classroom use is granted without fee provided that copies are not made or distributed for profit or commercial advantage and that copies bear this notice and the full citation on the first page. Copyrights for components of this work owned by others than the author(s) must be honored. Abstracting with credit is permitted. To copy otherwise, or republish, to post on servers or to redistribute to lists, requires prior specific permission and/or a fee. Request permissions from permissions@acm.org.

MM '25, October 27–31, 2025, Dublin, Ireland

© 2025 Copyright held by the owner/author(s). Publication rights licensed to ACM.

ACM ISBN 979-8-4007-2035-2/2025/10...\$15.00

<https://doi.org/10.1145/3746027.3755081>

(MM '25), October 27–31, 2025, Dublin, Ireland. ACM, New York, NY, USA, 13 pages. <https://doi.org/10.1145/3746027.3755081>

1 INTRODUCTION

Video generation has achieved significant progress in the recent few years, owing to the rapid development of the video diffusion model (VDM) [3, 58, 59]. Despite the promising advances in video diffusion quality, the high computational costs and slow inference time hinder the democratization of video generation tasks in real-world applications. For instance, generating a two-second video by Stable Video Diffusion [3] costs more than 25 seconds on an A100 GPU, and generating a 5 seconds video costs more than 5 minutes on online platforms such as KLing [1] and DreamMachine [37].

To address the computational challenges in VDM, two primary strategies can be adopted: reducing the number of sampling steps and decreasing model parameters. Recent research has predominantly focused on minimizing sampling steps. For instance, some works have extended consistency distillation techniques [13, 59, 63, 70], while other approaches have employed adversarial training methods [45, 72] to VDM. On the other hand, model compression techniques for VDM remain under-explored. While the common model compression techniques such as pruning [12, 18, 23, 27, 38, 53, 64] and knowledge distillation [5, 24] have shown promising results on image diffusion models [6, 33, 40], directly applying these methods to video diffusion models is still challenging.

First, unlike the image diffusion models, where block importance can be relatively easily estimated by assessing the quality of a single generated image, pruning in VDMs requires a more complex evaluation. In VDMs, it's essential to assess both the quality of content in individual frames and the motion dynamic consistency across the entire generated video [14, 15]. Through comprehensive analysis, we have observed that the deeper layers of VDMs are crucial for maintaining multi-frame content consistency, particularly in terms of motion dynamics across frames. In contrast, the shallower layers primarily contribute to the generation of individual RGB content in each frame. This insight allows us to selectively prune shallower layers while preserving the deeper ones, which optimizes computational efficiency without compromising video quality. With such observation, we present a light-weight VDM architecture **VDMini**, which achieves a $2.5 \times$ and $1.4 \times$ speedup for the image-to-video (I2V) and the text-to-video (T2V) generation tasks, respectively.

To further enhance the performance of the pruned VDM (i.e., VDMini) and achieve comparable generation quality to the unpruned VDM, we perform a post-pruning fine-tuning procedure. Given

This work was done during Yiming Wu's fellowship at The University of Hong Kong

*Zhenghao Chen and Dong Xu are the corresponding authors.

E-mail address: ymingwu, dongxu@hku.hk, zhenghao.chen@newcastle.edu.au and wanghuan@westlake.edu.cn

the aforementioned challenges, we focus on maintaining both individual content quality (i.e., spatial smoothness within a single frame) and motion dynamics quality (i.e., coherence across the entire video). To this end, we propose a novel Individual Content and Motion Dynamics (ICMD) Consistency Loss, which ensures consistency between the pruned VDMini (i.e., student) and the unpruned VDM (i.e., teacher). Drawing inspiration from prior work in image generation [33], we employ knowledge distillation to preserve individual content consistency. Additionally, to ensure multi-frame content consistency without redundancy, we introduce an adversarial loss on video-level feature representations, reinforcing overall content coherence.

We validate the effectiveness of our approach on two representative video generation tasks: Image-to-Video (I2V) and Text-to-Video (T2V) on the UCF101 and VBench benchmarks. By combining the proposed block pruning technique with the ICMD loss, our method achieves a $2.5\times$ speedup on the I2V model SF-V [72] and a $1.4\times$ speedup on the T2V model T2V-Turbo-V2 [39], while maintaining comparable generation quality. Moreover, for T2V tasks, we conducted additional experiments using the latest diffusion transformer-based T2V model, Hunyuan [35], achieving a 25% speedup and demonstrating generalizability. Our contributions are summarized as follows:

- We conduct a comprehensive assessment for the importance estimation of VDM blocks based on individual content and motion dynamics, followed by pruning the redundant layers to achieve model compression. To this end, we present a lightweight VDM variant VDMini, which achieves a significant speedup in inference time.
- To ensure quality consistency between the pruned VDMini and the unpruned VDM, we introduce the ICMD loss, it consists of two components: the ICD Loss for individual content consistency, which aligns the generated content in each single frame, and the MCA Loss for multi-frame content consistency, which preserves motion dynamics across the entire video. By maintaining frame-level and video-wide consistency, we can align VDMini with the unpruned VDM.
- We validate the effectiveness of our approach on two video generation tasks, namely I2V and T2V. Our method achieves a $2.5\times$ speedup over the I2V model SF-V and a $1.4\times$ (*resp.* $1.25\times$) speedup over the T2V model T2V-Turbo-v2 (*resp.* HunyuanVideo) while maintaining comparable quality metrics on the benchmarks UCF101, VBench-T2V, and VBench-I2V.

2 RELATED WORK

2.1 Video Generation

Video generation has seen wide exploration in recent years. Traditionally, generative adversarial networks (GANs) [21] and VAEs [34] have been utilized for this purpose, but they are generally limited to producing low-quality and short-duration videos. The advent of diffusion models and large-scale video datasets has significantly enhanced video generation quality. Initial explorations [32, 71] leverage pre-trained image models for video generation without the need for fine-tuning *i.e.* training-free methods. However, despite the reduction in training requirements, these approaches are

limited in terms of both inference speed and generation quality due to their reliance on DDIM Inversion [57].

With the emergence of large-scale video datasets such as WebVid-10M [2] and Panda70M [11], training-based methods have demonstrated significant improvements in generation quality and condition consistency capabilities. Jonathan *et al* [26] were the first to extend diffusion models to 3D space-time modeling by incorporating factorized space-time attention blocks into a U-Net architecture.

To leverage pre-trained image diffusion models, approaches such as Video LDM [4], Animatediff [22], VideoCrafter2 [9], and Stable Video Diffusion [3] have been developed. These methods introduce temporal layers following the residual and attention blocks of image generation models, and then employ multi-stage fine-tuning on high-quality video datasets, leading to substantial improvements in generation quality.

On the other hand, pure transformer-based models, such as DiT [52], originally designed for image generation, have also been adapted for video generation. Sora [51] achieved remarkable results by scaling up transformer-based architectures for video generation. To make advanced video generation models more accessible, Open-Sora [74] and Open-Sora-Plan [36] were introduced as open-source solutions for the community. Additionally, CogVideoX [69] proposed an Expert Transformer model for long-duration video generation, surpassing previous state-of-the-art methods. Recent works such as Snap Video [46], Mochi-1 [62], HunyuanVideo [35], and Wan2.1 [66] have also demonstrated impressive advancements in video generation tasks. Concurrently, methods like SF-V [72], AnimateLCM [63], OSV [45], and T2V-Turbo [39] focus on reducing inference steps to as few as one to four, albeit with some trade-offs in video quality.

Our approach aims to accelerate video generation by compressing existing high-cost models while preserving generation quality. Our work addresses two specific video generation tasks: image-to-video (I2V) and text-to-video (T2V), through our proposed lightweight model, VidMini, which achieves both efficiency and quality.

2.2 Pruning for Diffusion Models

The excessive size of diffusion models has prompted research on compressing diffusion models via two classic model compression techniques: network pruning, and distillation. Here we summarize the recent advances on them.

SnapFusion [40] stands out as an early contributor to accelerating diffusion models, employing two primary strategies: architectural refinement through pruning [18, 23, 38, 64], and reducing inference iterations via distillation [24, 47, 54]. Central to pruning efforts is effectively assessing the relative importance of model weights. To this end, SnapFusion proposes an importance metric based on two critical factors: reduction in CLIP score and improvement in latency. Specifically, they employ a prevalent trial-and-error approach [48, 49], systematically removing individual modules to measure associated impacts on CLIP scores and latency. Modules demonstrating minimal CLIP degradation alongside maximal latency improvement are identified as candidates for pruning. This approach yields a significantly streamlined UNet architecture that achieves a performance enhancement exceeding 7-fold compared to the original SD-v1.5 model.

For further inference optimization, SnapFusion introduces a CFG-aware distillation technique, ensuring the student model outputs closely match those of the teacher model post-CFG application. Consequently, SnapFusion attains an exceptional inference speed under 2 seconds on an iPhone 14 Pro, preserving the original model's CLIP and FID scores.

Concurrent to SnapFusion, BK-SDM [33] also attempts to accelerate SD models by pruning weight blocks. Unlike SnapFusion, their block importance analysis only considers CLIP score drop and they do not reduce the inference steps. Importantly, they propose a feature-distillation-based retraining strategy to regain model performance after pruning. Overall, BK-SDM achieves 30% to 50% reduction in model size and latency against the original SD model, with a small degradation in CLIP score and FID. The compact BK-SDM-Tiny model is further enhanced to EdgeFusion [7] by leveraging a strong teacher, LCM [44] to reduce inference steps, and high-quality AI-generated data.

MobileDiffusion [73] is a subsequent work that accelerates SD models by improving its architecture and reducing inference steps, too. Like SnapFusion and BK-SDM, it also utilizes pruning to remove redundant residual blocks. Differently, MobileDiffusion proposes even more fine-grained architecture optimizations, such as using more transformers in the middle of U-Net and fewer channels, decoupling self-attention from cross-attention, sharing key-value projections, using separable convolutions, and so on. For reducing inference steps, they adopt the distillation loss from prior works, SnapFusion [40] and UFOGen [68]. Overall, by integrating these optimization techniques, they achieve a remarkable inference speed of 0.2 second on an iPhone 15 Pro. SnapGen [10], another recent effort, pushes the boundary further by jointly redesigning the architecture and introducing adversarial-aware distillation strategies to support high-resolution image synthesis on mobile devices. It achieves strong generation quality using as few as 4 to 8 denoising steps while maintaining a lightweight model footprint. This line of work is extended to the video domain in SnapGen-V [67], a concurrent effort to ours, which introduces spatiotemporal attention mechanisms and temporally-aware distillation to support efficient video generation with competitive fidelity and temporal consistency on resource-constrained platforms.

In addition to the above works that aim to accelerate the SD models, some papers study the pruning methods on relatively small diffusion models. Diff-Pruning [19] prunes the channels of diffusion models by employing the dependency graph tool developed in DepGraph [18] to address the structural dependency problem when pruning models with residual connections. The method is shown to be effective on small-scale datasets with a max image resolution of 256×256, no SD models evaluated.

Our paper differs from the works above in that we focus on accelerating a practical *video* diffusion model, while the works above mainly focus on *image* diffusion models.

3 METHODOLOGY

3.1 Preliminaries

Diffusion Models. A diffusion model (DM) consists of two major processes: 1. a forward diffusion process that adds noise to the input data iteratively and 2. a reverse denoising process that removes the

predicted noise to recover the original input. In the continuous-time framework [30, 60], let $p(\mathbf{x}; \sigma)$ as the distribution obtained by adding Gaussian noise σ to the data distribution $p_{data}(\mathbf{x}_0)$. With a large σ_{max} , the distribution $p(\mathbf{x}; \sigma_{max})$ is close to the pure noise distribution. Then, the probability flow ordinary differential equation (PF-ODE) is defined as:

$$d\mathbf{x} = -\dot{\sigma}_t \sigma_t \nabla_{\mathbf{x}} \log p(\mathbf{x}, \sigma_t) dt, \quad (1)$$

where the score function $\nabla_{\mathbf{x}} \log p(\mathbf{x}, \sigma_t)$ is generally approximated by $\frac{D_{\theta}(\mathbf{x}, \sigma_t) - \mathbf{x}}{\sigma_t^2}$. In the EDM framework [30, 31], $D_{\theta}(\mathbf{x}_t, \sigma_t)$ is parameterized as follows:

$$D_{\theta} = c_0(t)\mathbf{x}_t + c_1(t)f_{\theta}(c_2(t)\mathbf{x}_t, c_3(t)), \quad (2)$$

where f_{θ} is the learnable neural network trained by minimizing denoising error, and c_0, c_1, c_2 , and c_3 are the time-dependent conditioning coefficients. The I2V models SF-V [72] and SVD [3] are developed based on the EDM framework.

Consistency Models. Consistency models (CM) [58, 59] offers a new family of generative models which enforces the learned neural network $f_{\theta}(\mathbf{x}_t, t)$ maps the arbitrary noise input \mathbf{x}_t to the clean data \mathbf{x}_0 , and the CM follows the self-consistency property $f_{\theta}(\mathbf{x}_t, t) = f_{\theta}(\mathbf{x}'_t, t')$, where \mathbf{x}'_t and \mathbf{x}_t represent the samples on the ODE trajectory at different times t and t' . Following the pre-conditioned EDM framework, the CM sets the boundary condition as $c_0(0) = 1$ and $c_1(0) = 0$.

One way to train the CM is to use consistency distillation, which distills the pre-trained DMs by minimizing the consistency loss:

$$\mathcal{L}_{CM}(\theta, \theta^-; \Psi) = \mathbb{E} \left[d \left(f_{\theta}(\mathbf{x}_{t_{n+k}}, t_{n+k}), f_{\theta^-}(\hat{\mathbf{x}}_{t_n}^{\Psi, \omega}, t_n) \right) \right], \quad (3)$$

where d is the distance function, $\hat{\mathbf{x}}_{t_n}^{\Psi, \omega}$ is the reversed data by ODE solver Ψ with classifier-free guidance (CFG) [25] weight ω , n is the time step for pretrained DM, and k is step interval. The T2V model T2V-Turbo-v2 [58] is developed based on the CM.

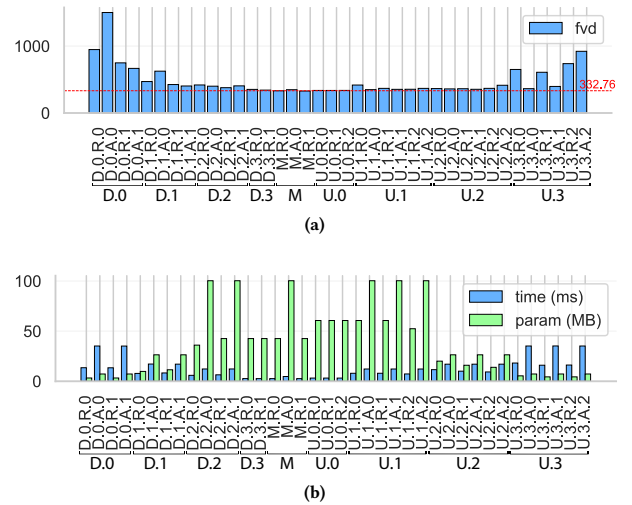


Figure 1: (a) FVD score by removing or replacing the blocks in the U-Net. (Note that a high FVD score means the block is more important.) (b) Time and Parameters of the blocks in the U-Net.

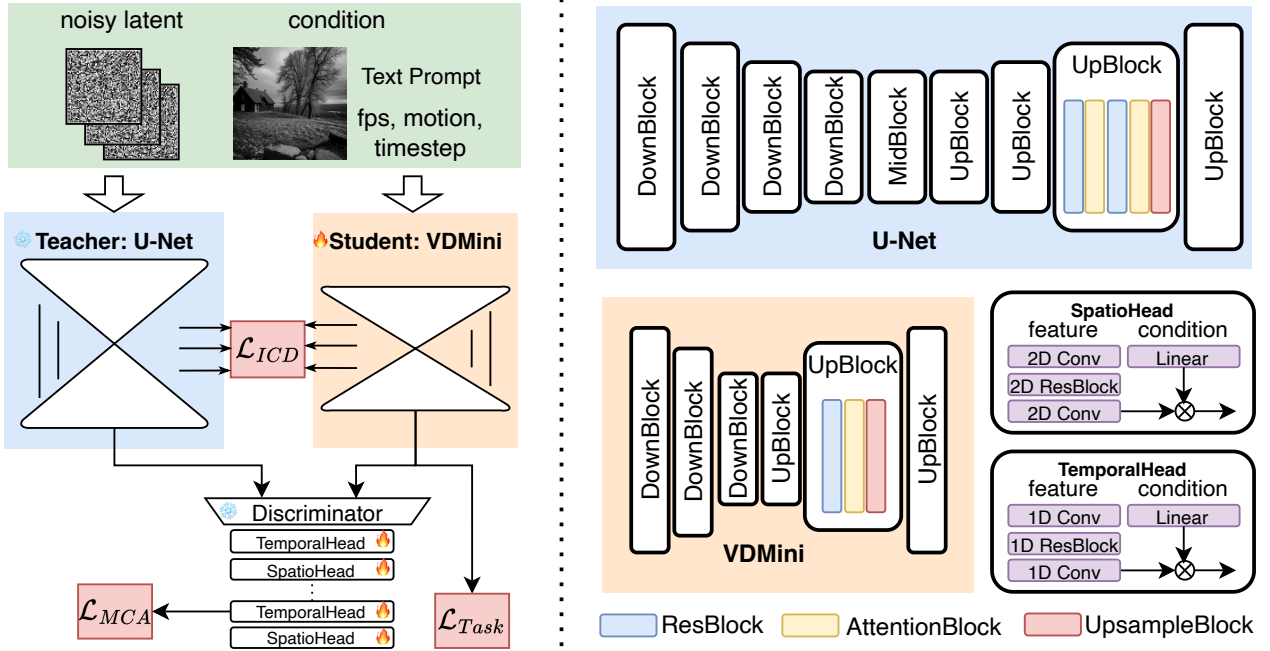


Figure 2: The proposed VDMini framework for Video Diffusion Model Compression. Left: The retraining process with the proposed ICMD loss, where \mathcal{L}_{ICD} is the knowledge distillation loss for individual content consistency, and \mathcal{L}_{MCA} is the adversarial loss for multi-frame content consistency. \mathcal{L}_{Task} is the task-specific loss function adopted in the base model. **Right:** The teacher model is pruned by blocks to obtain the student model (i.e., VDMini). The second Block (ResBlock, AttentionBlock) in the DownBlock and UpBlock are removed (Except for the second last DownBlock and UpBlock), and the innermost Blocks (MidBlock, DownBlock, and UpBlock) are entirely removed.

3.2 Network Pruning

Individual Content and Motion Dynamics Preserved Pruning.

Since the different network blocks play distinct roles in generating videos, we should assess the importance of blocks in both *individual content quality* and *motion dynamics*, followed by using the FVD score to quantify the block importance of the SF-V model.

By deconstructing the U-Net architecture, we assess the importance of each block by systematically replacing it with either an identity mapping or a single convolutional layer in cases where there is a channel mismatch. This approach allows us to isolate and evaluate the contribution of individual blocks. As illustrated in 1, “D”, “M”, and “U” denote the DownBlock, MidBlock, and UpBlock, respectively. For a specific block “D.0.R.1”, “R” and “A” represent ResBlock and AttentionBlock, respectively. The first number “0” and the second number “1” represent the block index and the layer index within the block, respectively. Our overall evaluation indicate that removing low-resolution layers in the U-Net significantly raises the FVD score, suggesting a substantial impact on the generation quality of individual frames. In contrast, removing high-resolution layers has a comparatively smaller effect on the FVD score, indicating that these layers are less critical to maintaining the generation quality of each individual frame. In addition to evaluating the individual frame generation quality, we also analyze the motion dynamics of the generated videos by visualizing the generated videos of the pruned U-Net. Our empirical observations reveal that removing the blocks in “D.2” and “U.1” significantly

affects the temporal coherence and motion dynamics across frames, leading to noticeable degradation in video quality.

In the end, we prune the second R-A pairs in the DownBlocks and UpBlocks except for the second last DownBlock “D.2” and the second UpBlock “U.1”, and further remove the MidBlock. Further visualization results and detailed analyses are provided in the supplement.

Compressed Network Architecture. In addition to the U-Net, we find that the VAE decoder used in SF-V significantly contributes to the inference time during the latent decoding process. To address this, we apply both layer pruning and channel pruning to the VAE decoder. Utilizing the introduced network pruning techniques, we develop lightweight VDMini models for I2V and T2V tasks, referred to as VDMini-I2V and VDMini-T2V. Finally, the pruned models demonstrate a 2.5× speedup for I2V model SF-V and a 1.4× speedup for T2V model T2V-Turbo-v2. We extend our compression technique and achieve a 1.25× speedup on the DiT-based T2V model, HunyuanVideo.

3.3 ICMD Consistency Loss

We aim to further enhance the generation performance of the pruned VDMini network by mimicking the intermediate outputs of the U-Net from the original VDM. As previously mentioned, in order to maintain the generation quality of individual frames and the motion dynamics across the video, we propose the Individual Content and Motion Dynamic (ICMD) Consistency Loss.

This optimization strategy consists of two parts: Individual Content Distillation (ICD) Loss and Multi-frame Content Adversarial (MCA) Loss. The proposed framework is illustrated in Figure 2.

Individual Content Distillation Loss: As illustrated in 2, ICD loss aims to achieve feature distillation [33] for each individual frame, which transfers the knowledge from the UNet of VDM (i.e., teacher model) to VDMini (i.e., student model). Formally, given a noisy video latent $\mathbf{x}_t \in R^{F \times C \times H \times W}$, the student model f_l^{stu} is trained by minimizing the distance of intermediate representations between the teacher model f_l^{tea} and the student model:

$$\mathcal{L}_{ICD} = \mathbb{E} \left[\sum_{l=1}^L d \left(f_l^{stu}(\mathbf{x}_t, t), f_l^{tea}(\mathbf{x}_t, t) \right) \right], \quad (4)$$

where L is the number of intermediate representation, and $f_l^{stu}(\cdot)$ and $f_l^{tea}(\cdot)$ denote the feature representations at the l -th block of the student and teacher models, respectively.

Multi-frame Content Adversarial Loss: With the ICD loss, the student model is forced to mimic the teacher model at the individual content level. However, the motion dynamics across the generated video can not be guaranteed. To address this issue, we introduce the MCA loss to adopt adversarial optimization strategy for preserving the motion dynamics across the generated video. Here, we let the discriminator D_ϕ to distinguish the video latent generated by the student model f^{stu} from the output of the teacher model f^{tea} as in Diffusion-GAN [65]. The discriminator D_ϕ comprises a combination of SpatioHead and TemporalHead components with standard 1D and 2D convolutional operations shown in Figure 2. We empirically observe that the temporal heads in the discriminator effectively enhance motion dynamics. Inspired by MCM and SF-V, we observe that the learnable MLP better captures motion in video generation tasks. Therefore, we incorporate these simple temporal heads to encode the motion information.

The optimization objective \mathcal{L}_{MCA} can be formulated as:

$$\begin{aligned} \mathcal{L}_{MCA}^{gen} &= -\mathbb{E} \left[\log \left(D_\phi(f^{stu}(\mathbf{x}_t, t)), \sigma_{t'} \right) \right], \\ \mathcal{L}_{MCA}^{disc} &= \mathbb{E} \left[\max(0, 1 + D_\phi(f^{stu}(\mathbf{x}_t), t), \sigma_{t'}) \right] \\ &\quad + \mathbb{E} \left[\max(0, 1 - D_\phi(f^{tea}(\mathbf{x}_t, t), \sigma_{t'})) \right], \end{aligned} \quad (5)$$

where $\sigma_{t'}$ is the instance noise injected into the samples at timestep t' , we follow SF-V to set the noise distribution as a discretized log-normal distribution, and $t' \in [1, 999]$. During SF-V fine-tuning, we incorporate both the teacher model and the original discriminator into the discriminator loss. This approach leverages real and synthetic samples from the teacher model to guide the score estimation of the denoiser, resulting in better performance in our experiments.

Along with our newly proposed ICMD loss, task-specific losses \mathcal{L}_{Task} are also incorporated during the fine-tuning process. Specifically, for the I2V task, SF-V employs a combination of reconstruction loss and adversarial loss. For the T2V task, T2V-Turbo-v2 utilizes a consistency loss along with a mixture of reward optimization objectives, and we further extend the proposed pruning and distillation method on the DiT-based T2V model HunyuanVideo [35], which trains a 13B model with the flow matching framework [43].

The final optimization objective is formulated as:

$$\mathcal{L} = \mathcal{L}_{Task} + \lambda_{ICD} \mathcal{L}_{ICD} + \lambda_{MCA} (\mathcal{L}_{MCA}^{gen} + \mathcal{L}_{MCA}^{disc}), \quad (6)$$

where λ_{ICD} and λ_{MCA} are the hyper-parameters to balance the ICD and MCA loss, respectively, the optimization details about task-specific losses for the I2V and T2V tasks are provided in the supplementary materials. During SF-V fine-tuning, we incorporate both the original task-specific loss \mathcal{L}_{Task} and the added \mathcal{L}_{ICD} and \mathcal{L}_{MCA} losses, the teacher model and the original discriminator are both utilized in the discriminator loss. This leverages real and synthetic samples from the teacher model to guide the score estimation of the denoiser, resulting in better performance in our experiments.

4 EXPERIMENTS

4.1 Datasets and Evaluation Metrics

Datasets: We utilize three datasets for training: OpenVid-1M [50], VidGen-1M [61], WebVid-10M [2] and HD-Mixkit [41]. OpenVid-1M and VidGen-1M are large-scale video datasets featuring high-quality videos and expressive captions, each containing over 1 million video-caption pairs. WebVid-10M is a widely-used video dataset collected from the web, encompassing diverse video content. For the I2V task, we first re-implement SF-V using the OpenVid-1M dataset, and then fine-tune the pruned VDMini-I2V model. For the T2V task, we follow the T2V-Turbo-v2 [39] setup, training the model on a dataset of VidGen-1M and WebVid-10M, comprising 180K video-text pairs. For fine-tuning the HunyuanVideo model, we adopt the implementation from FastVideo¹ and utilize a dataset comprising 1.2M samples from OpenVid-1M and HD-Mixkit.

Evaluation Metrics: We adopt the same evaluation metrics used in SF-V and T2V-Turbo-v2 for a fair comparison. Specifically, we use the FVD score [20] to measure the quality of the generated videos in the I2V task, which calculates the Fréchet Video Distance between the generated videos and the ground-truth videos from UCF101. Following SF-V, we use the first frame of the video as the conditional input to VDMini to generate the video with a resolution of 768×1024, then resize the video to 240×320 for evaluation. The videos are saved as 95% quality JPEG images, following the same setting in [56]. And we evaluate the I2V models on the comprehensive benchmark VBFench-I2V [29] to have a multi-dimensional evaluation. For the T2V task, we assess the performance of our model on VBFench-T2V [28], which automatically evaluates T2V models in terms of video quality and video prompt consistency, with a total of 16 diverse evaluation dimensions. We set the inference step to 16 for the T2V task, generating videos with a resolution of 320×512 and a video length of 16 for T2V-Turbo-v2, and the resolution for HunyuanVideo is 720p with 125 frames.

4.2 Implementation Details

In the experiments, we use 8 NVIDIA A100 GPUs for training the VDMini models and evaluate the models on a single A100 GPU. During the pruning stage, we evaluate the per-block FVD by replacing each block with either an identity block or a shortcut convolution layer regarding channel mismatch. We sample 1200 videos for evaluating in this stage, which takes around 9.5 hours on the server. For training the VDMini-I2V model, we set the resolution of the input video to 448×576. The model is trained with a batch size of 32 (with gradient accumulation of 4) for 10K steps, and the

¹<https://github.com/hao-ai-lab/FastVideo>

Table 1: Evaluation of VDMini-I2V on the VBench-I2V dataset. In this table, we compare the performance of the unpruned model SF-V and VDMini-I2V with and without the motion consistency loss \mathcal{L}_{MCA} . The metrics are divided into two categories: I2V subject and background consistency, and motion smoothness, dynamic degree, aesthetic quality, and imaging quality. The results show that VDMini-I2V achieves comparable performance to SF-V while being more efficient.

Models	I2V Subject ↑	I2V Background ↑	Subject Consistency ↑	Background Consistency ↑
SF-V	97.48%	97.59%	95.54%	96.63%
VDMini-I2V w/o \mathcal{L}_{MCA}	97.40%	97.36%	95.33%	96.12%
VDMini-I2V	97.51%	97.53%	95.59%	96.54%
Models	Motion Smoothness↑	Dynamic Degree↑	Aesthetic Quality↑	Imaging Quality↑
SF-V	98.11%	32.13%	59.89%	68.48%
VDMini-I2V w/o \mathcal{L}_{MCA}	96.84%	23.84%	57.85%	66.25%
VDMini-I2V	98.34%	33.10%	59.18%	67.99%

Table 2: Comparison with the existing methods. VDMini-I2V achieves a comparable FVD score with SF-V and 16-step SVD.

Methods	NFE ↓	FVD ↓	Model Size↓	Latency (ms)↓
SVD	25	163.43	1.5B	20126
SVD	16	183.98	1.5B	12880
AnimateLCM	8	320.71	1.5B	7346
SF-V	1	166.26	1.5B	512
VDMini-I2V	1	198.13	940M	345

Table 3: Comparison with other baseline pruning approaches. DepGraph [18] explicitly models the dependency between layers and comprehensively groups coupled parameters for pruning, while Magnitude Pruning aims to remove the smallest magnitude weights in the network. L2 and Taylor are the criteria for importance estimation.

Methods	FVD ↓	Latency (ms) ↓
DepGraph (L2)	288.79	433
DepGraph (Taylor)	292.18	425
Magnitude Pruning (L2)	271.55	412
Magnitude Pruning (Taylor)	354.51	430
VDMini-I2V	198.13	345

MCA loss is enabled after 3K steps. The learning rate for the U-Net and the discriminator is set to 1e-4 and 1e-5, respectively. The VAE decoder is trained with a batch size of 8 for 15K steps. The frame length is sampled from 14 to 25, and the learning rate is initially set to 5e-5 and decayed using a cosine annealing schedule. The loss weights for reconstruction loss, perceptual loss, and adversarial loss are set to 1, 1, and 0.2, respectively. For training the VDMini-T2V model based on T2V-Turbo-v2, the resolution of the input video is set to 320×512 . We set the batch size for fine-tuning to 2 with 8K steps of gradient updating, and the learning rate for the discriminator is set to 1e-5. All other hyper-parameters are kept the same as in the T2V-Turbo-v2 training. The loss weights for ICD loss and MCA loss are set to 0.1 and 1, respectively. More details about training VDMini-T2V model based on HunyuanVideo are presented in the supplement.

4.3 Quantitative Results

Comparison with Other I2V Methods. To evaluate the performance of VDMini-I2V, we compare it with several state-of-the-art I2V models, including SF-V [56], SVD [3], and AnimateLCM [63]. The results are reported in Table 2 and Table 1.

As reported in Table 2, VDMini-I2V compresses the U-Net by approximately 40% in terms of parameters and achieves an FVD score of 198.13 after retraining, with no significant drop compared to the teacher model (*i.e.*, SF-V). When compared to SVD with 16 steps, VDMini-I2V achieves a similar FVD score but is much faster, with a 37× speedup. This substantial speedup is due to the pruning and fine-tuning strategy employed by VDMini, which reduces the computational complexity of the model without compromising the quality of the generated videos. The reduction in parameters not only accelerates inference time but also decreases the memory footprint, making VDMini-I2V more suitable for deployment in resource-constrained environments. Additionally, the retraining process ensures that the pruned model regains high fidelity in video generation, maintaining the visual quality and temporal coherence of the output videos. This balance between efficiency and performance highlights the practical advantages of VDMini-I2V over other SoTA methods.

Except for the evaluation on the UCF101 dataset, we further evaluate the performance of VDMini-I2V on the VBench-I2V benchmark [29], which provides a comprehensive evaluation of I2V models across multiple dimensions. As reported in Table 1, we observe that VDMini-I2V achieves competitive performance across various subjects, backgrounds, and motion-related metrics. The results indicate that VDMini-I2V effectively preserves the quality of the generated videos while significantly reducing the model size and inference time. This demonstrates the effectiveness of our proposed method in enhancing the performance of I2V models. The results of the motion-related metrics, **Motion Smoothness** and **Dynamic Degree**, in Table 1 present that \mathcal{L}_{MCA} effectively preserves motion dynamics during retraining. VDMini-I2V demonstrates competitive performance compared to the unpruned model SF-V, particularly excelling in motion-related metrics such as Motion Smoothness and Dynamic Degree.

Comparison with Other Baseline Pruning Methods. To further validate the effectiveness of the proposed VDMini method, we compare its performance with other structural pruning methods, including Magnitude-based pruning [38] and DepGraph [18].



Figure 3: Qualitative results of VDMini-I2V based on SVD. From top to bottom, the rows correspond to videos generated by SVD (25 steps), AnimateLCM (8 steps), SF-V (1 step), and VDMini-I2V (1 step). For each video, the leftmost image is the prompt image. From left to right: the 1st frame, the 10th frame, and the video are shown. *Best viewed with Acrobat Reader for animation. Click the last image to play the animation clips.*

Magnitude-based pruning focuses on removing the smallest magnitude weights in the network, while DepGraph constructs a dependency graph for the network and iteratively prunes model weights with low-importance scores, using the L2 Norm and first-order Taylor expansion of loss as the importance score. As shown in Table 3, our block pruning approach achieves faster latency than these methods for the same model size, primarily because most inference time is spent on high-resolution layers, such as the first DownBlock and the last UpBlock. Since the importance scores used by these pruning methods are not directly correlated with the evaluation protocol, the pruned network architecture may be suboptimal. With the same retraining process, VDMini-I2V achieves a better FVD score compared to these pruning methods.

Table 4: Effectiveness of loss components. Individual Content Distillation Loss (\mathcal{L}_{ICD}) and Integrated Content Adversarial Loss (\mathcal{L}_{ICA}) in the VDMini-I2V model.

\mathcal{L}_{ICD}	\mathcal{L}_{MCA}	FVD \downarrow
\times	\times	299.44
\checkmark	\times	224.24
\times	\checkmark	257.99
\checkmark	\checkmark	198.13

Effectiveness of the ICMD Loss. We conduct ablation studies to validate the effectiveness of the ICMD loss used during the fine-tuning stage. As shown in Table 4, enabling \mathcal{L}_{ICD} and \mathcal{L}_{MCA} individually results in FVD scores of 224.24 and 257.99, respectively. When both \mathcal{L}_{ICD} and \mathcal{L}_{MCA} are combined, the FVD score improves significantly to 198.13. These results highlight the substantial contribution of the ICMD loss to the overall performance of the model.

Table 5: Sensitivity analysis of hyperparameters λ_{ICD} and λ_{MCA} , representing the loss weights for \mathcal{L}_{ICD} and \mathcal{L}_{ICA} in the VDMini-I2V model.

λ_{ICD}	λ_{MCA}	FVD \downarrow
1	1	254.30
0.01	1	286.42
0.1	0.5	198.63
0.1	1	198.13

Effectiveness of Loss Weight. To balance the ICMD loss with the task-specific loss during the training stage, we perform experiments with different hyper-parameters λ_{ICD} and λ_{MCA} . As shown in Table 5, we find that the result is sensitive to λ_{ICD} , while more robust to λ_{MCA} . The best result is obtained when λ_{ICD} and λ_{MCA} are set to 0.1 and 1, respectively. This indicates that careful tuning of these hyper-parameters is crucial for optimizing the performance of the model.

Table 6: Comparison of VDMini-T2V with other methods on VBFench-T2V in terms of Quality Score, Semantic Score, Total Score, and Latency.

Methods	Quality \uparrow	Semantic \uparrow	Total \uparrow	Latency (ms) \downarrow
UNet-based Model				
Kling	83.39	75.68	81.85	-
VideoCrafter2	82.20	73.42	80.44	-
T2V-Turbo-v2	85.13	77.12	83.52	2554.05
VDMini-T2V-Turbo	83.33	77.38	82.14	1662.26
DiT-based Model				
FastVideo	85.09	75.82	83.24	366.11
VDMini-T2V-HY	84.34	74.76	82.42	292.89

Comparison with Other T2V models. On the other hand, we apply the proposed pruning and fine-tuning strategy on UNet-based T2V-Turbo-v2 and DiT-based HunyuanVideo, resulting in VDMini-T2V. As shown in Table 6, we find that VDMini-T2V (T2V-Turbo-v2) reduces 35% inference time compared to T2V-Turbo-v2, with a small degradation on Quality Score after retraining. However, the VDMini-T2V still achieves better results compared to the other models, such as VideoCrafter2 and Kling. Besides, we conduct experiments on DiT-based model HunyuanVideo by pruning the Dual-stream blocks from **20** to **12** and the Single-stream blocks from **40** to **28**, resulting in only a marginal performance drop of 0.82%



Figure 4: Qualitative Results of VDMini-T2V. For the first two rows, the Prompt is An astronaut flying in space, surrealism style. The first row shows the video generated by T2V-Turbo-v2, while the second row presents the video generated by VDMini-T2V-Turbo. For the last two rows, the Prompt is A hand with delicate fingers The third row displays the video generated by HunyuanVideo, and the fourth row shows the video generated by VDMini-T2V-HY based on HunyuanVideo. From left to right: the 1st frame, the 10th frame, and the video are shown. *Best viewed with Acrobat Reader for animation. Click the last image to play the animation clips.*

on VBench-T2V, while achieving a $1.25\times$ speed up, the inference speed is tested on a single A100 GPU.

4.4 Qualitative Results

Visual Results on the I2V Task. As shown in Figure 3, the generated results of our method and other related approaches in the I2V task demonstrate satisfactory performance. The visual results indicate that our method effectively maintains both individual and multi-frame content consistency across frames, preserving similar styles and motions as the teacher model SF-V. In contrast, other methods suffer from blurring or distortion due to motion. Our method exhibits high visual quality and smooth motion with only one step inference.

Visual Results on the T2V task. We also present the visual results of the VDMini-T2V models in Figure 4. The generated videos demonstrate that the VDMini-T2V model is capable of producing high-quality videos that accurately reflect a wide range of input text prompts. The visual consistency and fidelity of the generated videos highlight the effectiveness of our proposed method, ensuring that the VDMini-T2V model maintains the integrity and coherence of the video content while significantly reducing inference time.

5 CONCLUSION

In this work, we have presented VDMini, a lightweight Video Diffusion Models (VDMs). Our approach concentrates on reducing the inference time while maintaining the individual content and multi-frame content quality. The pruning strategy is designed by analyzing the importance of the blocks in the U-Net as well as the visual quality of the generated video, leading to the removal of redundant shallower layers and preserving the deeper layers to keep the quality of multi-frame content. To further enhance the motion dynamics and quality of the generated video, we apply a multi-frame content adversarial loss with individual content distillation loss during the fine-tuning process. We achieve an average $2.5\times$, $1.4\times$, and $1.25\times$ speed up for the I2V method SF-V, the T2V method T2V-Turbo-v2, and the T2V method HunyuanVideo, respectively.

REFERENCES

- [1] Kling AI. 2023. Kling AI. <https://klingai.com/>.
- [2] Max Bain, Arsha Nagrani, Gùl Varol, and Andrew Zisserman. 2021. Frozen in time: A joint video and image encoder for end-to-end retrieval. In *Proc. IEEE Conf. CVPR*. 1728–1738.
- [3] Andreas Blattmann, Tim Dockhorn, Sumith Kulal, Daniel Mendelevitch, Maciej Kilian, Dominik Lorenz, Yam Levi, Zion English, Vikram Voleti, Adam Letts,

et al. 2023. Stable video diffusion: Scaling latent video diffusion models to large datasets. *arXiv preprint arXiv:2311.15127* (2023).

[4] Andreas Blattmann, Robin Rombach, Huan Ling, Tim Dockhorn, Seung Wook Kim, Sanja Fidler, and Karsten Kreis. 2023. Align your latents: High-resolution video synthesis with latent diffusion models. In *Proc. IEEE Conf. CVPR*. 22563–22575.

[5] Cristian Bucilă, Rich Caruana, and Alexandru Niculescu-Mizil. 2006. Model compression.

[6] Thibault Castells, Hyoung-Kyu Song, Tairen Piao, Shinkook Choi, Bo-Kyeong Kim, Hanyoung Yim, Changgwun Lee, Jae Gon Kim, and Tae-Ho Kim. 2024. Edge-Fusion: On-Device Text-to-Image Generation. *arXiv preprint arXiv:2404.11925* (2024).

[7] Thibault Castells, Hyoung-Kyu Song, Tairen Piao, Shinkook Choi, Bo-Kyeong Kim, Hanyoung Yim, Changgwun Lee, Jae Gon Kim, and Tae-Ho Kim. 2024. Edge-Fusion: On-Device Text-to-Image Generation. *arXiv preprint arXiv:2404.11925* (2024).

[8] Haixin Chen, Menghan Xia, Yingqing He, Yong Zhang, Xiaodong Cun, Shaoshu Yang, Jinbo Xing, Yaofang Liu, Qifeng Chen, Xintao Wang, et al. 2023. Videocrafter1: Open diffusion models for high-quality video generation. *arXiv preprint arXiv:2310.1512* (2023).

[9] Haixin Chen, Yong Zhang, Xiaodong Cun, Menghan Xia, Xintao Wang, Chao Weng, and Ying Shan. 2024. Videocrafter2: Overcoming data limitations for high-quality video diffusion models. In *Proc. IEEE Conf. CVPR*. 7310–7320.

[10] Jierun Chen, Dongting Hu, Xijie Huang, Huseyin Coskun, Arpit Sahni, Aarush Gupta, Anujraaj Goyal, Dishani Lahiri, Rajesh Singh, Yerlan Idelbayev, et al. 2025. Snapgen: Taming high-resolution text-to-image models for mobile devices with efficient architectures and training. In *Proc. IEEE Conf. CVPR*. 7997–8008.

[11] Tsai-Shien Chen, Aliaksandr Siarohin, Willi Menapace, Ekaterina Deyneka, Hsiang-wei Chao, Byung Eun Jeon, Yuwei Fang, Hsin-Ying Lee, Jian Ren, Ming-Hsuan Yang, and Sergey Tulyakov. 2024. Panda-70M: Captioning 70M Videos with Multiple Cross-Modality Teachers. In *Proc. IEEE Conf. CVPR*.

[12] Zhenghao Chen, Shuhang Gu, Guo Lu, and Dong Xu. 2022. Exploiting intra-slice and inter-slice redundancy for learning-based lossless volumetric image compression. *IEEE Transactions on Image Processing* 31 (2022), 1697–1707.

[13] Zhenghao Chen, Guo Lu, Zhihao Hu, Shan Liu, Wei Jiang, and Dong Xu. 2022. L SVC: A learning-based stereo video compression framework. In *Proc. IEEE Conf. CVPR*. 6073–6082.

[14] Zhenghao Chen, Lucas Relic, Roberto Azevedo, Yang Zhang, Markus Gross, Dong Xu, Luping Zhou, and Christopher Schroers. 2023. Neural video compression with spatio-temporal cross-covariance transformers. In *Proc. ACM Multimedia*. 8543–8551.

[15] Zhenghao Chen, Luping Zhou, Zhihao Hu, and Dong Xu. 2024. Group-aware parameter-efficient updating for content-adaptive neural video compression. In *Proc. ACM Multimedia*. 11022–11031.

[16] Patrick Esser, Sumith Kulal, Andreas Blattmann, Rahim Entezari, Jonas Müller, Harry Saini, Yam Levi, Dominik Lorenz, Axel Sauer, Frederic Boesel, et al. 2024. Scaling rectified flow transformers for high-resolution image synthesis. In *Proc. ICML*.

[17] Patrick Esser, Robin Rombach, and Björn Ommer. 2021. Taming transformers for high-resolution image synthesis. In *Proc. IEEE Conf. CVPR*. 12873–12883.

[18] Gongfan Fang, Xinyi Ma, Mingli Song, Michael Bi Mi, and Xinchao Wang. 2023. DepGraph: Towards Any Structural Pruning. In *Proc. IEEE Conf. CVPR*.

[19] Gongfan Fang, Xinyi Ma, and Xinchao Wang. 2023. Structural Pruning for Diffusion Models. In *Proc. NeurIPS*.

[20] Songwei Ge, Aniruddha Mahapatra, Gaurav Parmar, Jun-Yan Zhu, and Jia-Bin Huang. 2024. On the Content Bias in Fréchet Video Distance. In *Proc. IEEE Conf. CVPR*. 7277–7288.

[21] Ian Goodfellow, Jean Pouget-Abadie, Mehdi Mirza, Bing Xu, David Warde-Farley, Sherjil Ozair, Aaron Courville, and Yoshua Bengio. 2020. Generative adversarial networks. *Commun. ACM* 63, 11 (2020), 139–144.

[22] Yuwei Guo, Ceyuan Yang, Anyi Rao, Zhengyang Liang, Yaohui Wang, Yu Qiao, Maneesh Agrawala, Dahua Lin, and Bo Dai. 2024. AnimateDiff: Animate Your Personalized Text-to-Image Diffusion Models without Specific Tuning. In *Proc. ICLR*.

[23] Song Han, Jeff Pool, John Tran, and William J. Dally. 2015. Learning both weights and connections for efficient neural network. In *Proc. NeurIPS*.

[24] Geoffrey Hinton, Oriol Vinyals, and Jeff Dean. 2014. Distilling the knowledge in a neural network. In *Proc. NeurIPS Workshop*.

[25] Jonathan Ho and Tim Salimans. 2021. Classifier-Free Diffusion Guidance. In *Proc. NeurIPS Workshop*.

[26] Jonathan Ho, Tim Salimans, Alexey Gritsenko, William Chan, Mohammad Norouzi, and David J. Fleet. 2022. Video diffusion models. In *Proc. NeurIPS*, Vol. 35. 8633–8646.

[27] Torsten Hoefler, Dan Alistarh, Tal Ben-Nun, Nikoli Dryden, and Alexandra Peste. 2021. Sparsity in Deep Learning: Pruning and growth for efficient inference and training in neural networks. *JMLR* 22, 241 (2021), 1–124.

[28] Ziqi Huang, Yinan He, Jiashuo Yu, Fan Zhang, Chenyang Si, Yuming Jiang, Yuanhan Zhang, Tianxing Wu, Qingyang Jin, Nattapol Chanpaisit, Yaohui Wang, Xinyuan Chen, Limin Wang, Dahua Lin, Yu Qiao, and Ziwei Liu. 2024. VBench: Comprehensive Benchmark Suite for Video Generative Models. In *Proc. IEEE Conf. CVPR*.

[29] Ziqi Huang, Fan Zhang, Xiaojie Xu, Yinan He, Jiashuo Yu, Ziyue Dong, Qianli Ma, Nattapol Chanpaisit, Chenyang Si, Yuming Jiang, et al. 2024. Vbench++: Comprehensive and versatile benchmark suite for video generative models. *arXiv preprint arXiv:2411.13503* (2024).

[30] Tero Karras, Miika Aittala, Timo Aila, and Samuli Laine. 2022. Elucidating the design space of diffusion-based generative models. In *Proc. NeurIPS*, Vol. 35. 26565–26577.

[31] Tero Karras, Miika Aittala, Jaakko Lehtinen, Janne Hellsten, Timo Aila, and Samuli Laine. 2024. Analyzing and improving the training dynamics of diffusion models. In *Proc. IEEE Conf. CVPR*. 24174–24184.

[32] Levon Khachatryan, Andranik Movsisyan, Vahram Tadevosyan, Roberto Henschel, Zhangyang Wang, Shant Navasardyan, and Humphrey Shi. 2023. Text2video-zero: Text-to-image diffusion models are zero-shot video generators. In *Proc. IEEE Conf. CVPR*. 15954–15964.

[33] Bo-Kyeong Kim, Hyoung-Kyu Song, Thibault Castells, and Shinkook Choi. 2024. BK-SDM: A Lightweight, Fast, and Cheap Version of Stable Diffusion. In *Proc. ECCV*.

[34] Diederik P. Kingma. 2013. Auto-encoding variational bayes. *arXiv preprint arXiv:1312.6114* (2013).

[35] Weijie Kong, Qi Tian, Zijian Zhang, Rox Min, Zuozhuo Dai, Jin Zhou, Jiangfeng Xiong, Xin Li, Bo Wu, Jianwei Zhang, et al. 2024. Hunyuandvideo: A systematic framework for large video generative models. *arXiv preprint arXiv:2412.03603* (2024).

[36] PKU-Yuan Lab and Tuzhan AI etc. 2024. Open-Sora-Plan. doi:10.5281/zenodo.10948109

[37] Luma Labs. 2024. Dream Machine. <https://lumalabs.ai/dream-machine>.

[38] Hao Li, Asim Kadav, Igor Durdanovic, Hanan Samet, and Hans Peter Graf. 2017. Pruning filters for efficient convnets. In *Proc. ICLR*.

[39] Jiachen Li, Qian Long, Jian Zheng, Xiaofeng Gao, Robinson Piramuthu, Wenhui Chen, and William Yang Wang. 2024. T2V-Turbo-v2: Enhancing Video Generation Model Post-Training through Data, Reward, and Conditional Guidance Design. *arXiv preprint arXiv:2410.05677* (2024).

[40] Yanyu Li, Huan Wang, Qing Jin, Ju Hu, Pavlo Chemerys, Yun Fu, Yanzhi Wang, Sergey Tulyakov, and Jian Ren. 2023. SnapFusion: Text-to-Image Diffusion Model on Mobile Devices within Two Seconds. In *Proc. NeurIPS*.

[41] Bin Lin, Yunyang Ge, Xinhua Cheng, Zongjian Li, Bin Zhu, Shaodong Wang, Xianyi He, Yang Ye, Shanghai Yuan, Liuhan Chen, et al. 2024. Open-sora plan: Open-source large video generation model. *arXiv preprint arXiv:2412.00131* (2024).

[42] Pengyang Ling, Jiazi Bu, Pan Zhang, Xiaoyi Dong, Yuhang Zang, Tong Wu, Huaian Chen, Jiaqi Wang, and Yi Jin. 2024. MotionClone: Training-Free Motion Cloning for Controllable Video Generation. *arXiv preprint arXiv:2406.05338* (2024).

[43] Yaron Lipman, Ricky TQ Chen, Heli Ben-Hamu, Maximilian Nickel, and Matthew Le. 2023. Flow Matching for Generative Modeling. In *Proc. ICLR*.

[44] Simian Luo, Yiqin Tan, Longbo Huang, Jian Li, and Hang Zhao. 2023. Latent consistency models: Synthesizing high-resolution images with few-step inference. *arXiv preprint arXiv:2310.04378* (2023).

[45] Xiaofeng Mao, Zhengkai Jiang, Fu-Yun Wang, Wenbing Zhu, Jiangning Zhang, Hao Chen, Mingmin Chi, and Yabiao Wang. 2024. Osv: One step is enough for high-quality image to video generation. In *Proc. IEEE Conf. CVPR*.

[46] Willi Menapace, Aliaksandr Siarohin, Ivan Skorokhodov, Ekaterina Deyneka, Tsai-Shien Chen, Anil Kag, Yuwei Fang, Aleksei Stolar, Elisa Ricci, Jian Ren, et al. 2024. Snap video: Scaled spatiotemporal transformers for text-to-video synthesis. In *Proc. IEEE Conf. CVPR*. 7038–7048.

[47] Chenlin Meng, Ruiqi Gao, Diederik P. Kingma, Stefano Ermon, Jonathan Ho, and Tim Salimans. 2023. On distillation of guided diffusion models. In *Proc. IEEE Conf. CVPR*.

[48] Pavlo Molchanov, Stephen Tyree, Tero Karras, Timo Aila, and Jan Kautz. 2017. Pruning Convolutional Neural Networks for Resource Efficient Inference. In *Proc. ICLR*.

[49] Michael C. Mozer and Paul Smolensky. 1988. Skeletonization: A technique for trimming the fat from a network via relevance assessment. In *Proc. NeurIPS*.

[50] Kepan Nan, Rui Xie, Penghao Zhou, Tiehan Fan, Zhenheng Yang, Zhijie Chen, Xiang Li, Jian Yang, and Ying Tai. 2024. Openvid-1m: A large-scale high-quality dataset for text-to-video generation. *arXiv preprint arXiv:2407.02371* (2024).

[51] OpenAI. 2024. Sora. <https://openai.com/index/video-generation-models-as-world-simulators/>.

[52] William Peebles and Saining Xie. 2023. Scalable Diffusion Models with Transformers. *Proc. IEEE Conf. ICCV*.

[53] Russell Reed. 1993. Pruning algorithms - a survey. *IEEE transactions on Neural Networks* 4, 5 (1993), 740–747.

[54] Tim Salimans and Jonathan Ho. 2022. Progressive Distillation for Fast Sampling of Diffusion Models. In *Proc. ICLR*.

[55] Axel Sauer, Frederic Boesel, Tim Dockhorn, Andreas Blattmann, Patrick Esser, and Robin Rombach. 2024. Fast high-resolution image synthesis with latent adversarial diffusion distillation. 1–11.

[56] Ivan Skorokhodov, Sergey Tulyakov, and Mohamed Elhoseiny. 2022. Stylegan-v: A continuous video generator with the price, image quality and perks of stylegan. In Proc. IEEE Conf. CVPR. 3626–3636.

[57] Jiaming Song, Chenlin Meng, and Stefano Ermon. 2021. Denoising diffusion implicit models. Proc. ICLR.

[58] Yang Song and Prafulla Dhariwal. 2024. Improved Techniques for Training Consistency Models. In Proc. ICLR.

[59] Yang Song, Prafulla Dhariwal, Mark Chen, and Ilya Sutskever. 2023. Consistency Models. In Proc. ICML. 127–144. doi:10.1007/978-1-4842-1329-2_9

[60] Yang Song, Jascha Sohl-Dickstein, Diederik P Kingma, Abhishek Kumar, Stefano Ermon, and Ben Poole. 2021. Score-Based Generative Modeling through Stochastic Differential Equations. In Proc. ICLR. <https://openreview.net/forum?id=PxTiG12RRHS>

[61] Zhiyu Tan, Xiaomeng Yang, Luozheng Qin, and Hao Li. 2024. VidGen-1M: A Large-Scale Dataset for Text-to-video Generation. arXiv preprint arXiv:2408.02629 (2024).

[62] Genmo Team. 2024. Mochi 1. <https://github.com/genmoai/models>.

[63] Fu-Yun Wang, Zhaoyang Huang, Xiaoyu Shi, Weikang Bian, Guanglu Song, Yu Liu, and Hongsheng Li. 2024. AnimateLCM: Computation-Efficient Personalized Style Video Generation without Personalized Video Data. SIGGRAPH ASIA TCS.

[64] Huan Wang, Can Qin, Yulun Zhang, and Yun Fu. 2021. Neural Pruning via Growing Regularization. In Proc. ICLR.

[65] Zhendong Wang, Huangjie Zheng, Pengcheng He, Weizhu Chen, and Mingyuan Zhou. 2023. Diffusion-GAN: Training GANs with Diffusion. In Proc. ICLR.

[66] WanTeam, Ang Wang, Baole Ai, Bin Wen, Chaojie Mao, Chen-Wei Xie, Di Chen, Fei Yu, Haiming Zhao, Jianxiao Yang, Jianyuan Zeng, Jiayu Wang, Jingfeng Zhang, Jingren Zhou, Jinkai Wang, Jixuan Chen, Kai Zhu, Kang Zhao, Keyu Yan, Lianghua Huang, Mengyang Feng, Ningyi Zhang, Pandeng Li, Pingyu Wu, Ruihang Chu, Ruili Feng, Shiwei Zhang, Siyang Sun, Tao Fang, Tianxing Wang, Tianyi Gui, Tingyu Weng, Tong Shen, Wei Lin, Wei Wang, Wei Wang, Wenmeng Zhou, Wente Wang, Wenting Shen, Wenyuan Yu, Xianzhong Shi, Xiaoming Huang, Xin Xu, Yan Kou, Yangyu Lv, Yifei Li, Yijing Liu, Yiming Wang, Yingya Zhang, Yitong Huang, Yong Li, You Wu, Yu Liu, Yulin Pan, Yun Zheng, Yuntao Hong, Yupeng Shi, Yutong Feng, Zeyinzi Jiang, Zhen Han, Zhi-Fan Wu, and Ziyu Liu. 2025. Wan: Open and Advanced Large-Scale Video Generative Models. arXiv preprint arXiv:2503.20314 (2025).

[67] Yushu Wu, Zhixing Zhang, Yanyu Li, Yanwu Xu, Anil Kag, Yang Sui, Huseyin Coskun, Ke Ma, Aleksei Lebedev, Ju Hu, et al. 2025. Snapgen-v: Generating a five-second video within five seconds on a mobile device. In Proc. IEEE Conf. CVPR. 2479–2490.

[68] Yanwu Xu, Yang Zhao, Zhisheng Xiao, and Tingbo Hou. 2024. Ufogen: You forward once large scale text-to-image generation via diffusion gans. In Proc. IEEE Conf. CVPR.

[69] Zhuoyi Yang, Jiayan Teng, Wendi Zheng, Ming Ding, Shiyu Huang, Jiazheng Xu, Yuanming Yang, Wenyi Hong, Xiaohan Zhang, Guanyu Feng, et al. 2024. CogVideoX: Text-to-Video Diffusion Models with An Expert Transformer. arXiv preprint arXiv:2408.06072 (2024).

[70] Yuanhao Zhai, Kevin Lin, Zhengyuan Yang, Linjie Li, Jianfeng Wang, Chung-Ching Lin, David Doermann, Junsong Yuan, and Lijuan Wang. [n. d.]. Motion Consistency Model: Accelerating Video Diffusion with Disentangled Motion-Appearance Distillation. In Proc. NeurIPS.

[71] Yabo Zhang, Yuxiang Wei, Dongsheng Jiang, XIAOPENG ZHANG, Wangmeng Zuo, and Qi Tian. 2024. ControlVideo: Training-free Controllable Text-to-video Generation. In Proc. ICLR.

[72] Zhixing Zhang, Yanyu Li, Yushu Wu, Yanwu Xu, Anil Kag, Ivan Skorokhodov, Willi Menapace, Aliaksandr Siarohin, Junli Cao, Dimitris Metaxas, et al. 2024. SF-V: Single Forward Video Generation Model. In Proc. NeurIPS.

[73] Yang Zhao, Yanwu Xu, Zhisheng Xiao, and Tingbo Hou. 2023. Mobilediffusion: Subsecond text-to-image generation on mobile devices. arXiv preprint arXiv:2311.16567 (2023).

[74] Zangwei Zheng, Xiangyu Peng, Tianji Yang, Chenhui Shen, Shenggui Li, Hongxin Liu, Yukun Zhou, Tianyi Li, and Yang You. 2024. Open-Sora: Democratizing Efficient Video Production for All. <https://github.com/hpcfaitech/Open-Sora>

This appendix provides details about Section A, the compression of the VAE decoder of SF-V; Section B, the compressed U-Net; Section C, I2V and T2V baselines; Section D, the extensive experiments on the DiT-based HunyuanVideo.

A COMPRESSION OF THE VAE DECODER OF SF-V

The VAE decoder in the I2V method SF-V incurs significant inference time. Therefore, we follow [40] to apply both layer pruning

and channel pruning techniques [18] to compress the VAE decoder, which will further reduce the inference time for SF-V. Initially, we present the block-wise architecture of the VAE decoder in Figure A1 and the block-wise inference time and the number of parameters in Figure A2. Our observations indicate that the latter layers of the VAE decoder, which handle higher resolution features, consume most of the inference time. Specifically, we remove layers in the “MidBlock” and “UpBlock.3”, as these layers significantly contribute to inference time and model weight. Subsequently, we utilize Torch-Pruning [18] for channel pruning to further accelerate the model. This results in a compressed VAE decoder with a 70% reduction in inference time and a 30% reduction in the number of parameters. By fine-tuning the compressed VAE decoder on the OpenVid-1M dataset [50] using reconstruction loss, perceptual loss, and adversarial loss, we achieve performance comparable to the original VAE decoder.

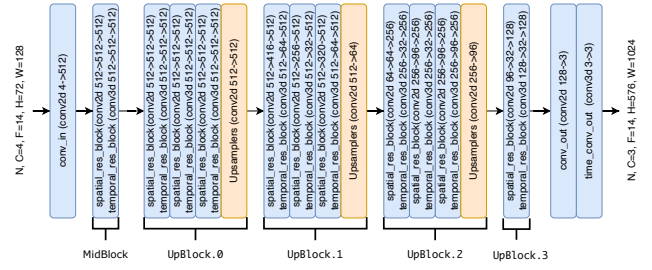


Figure A1: Network architecture of the compressed VAE decoder. First, we remove the layers in MidBlock and UpBlock.3, then perform channel pruning to speed up inference time.

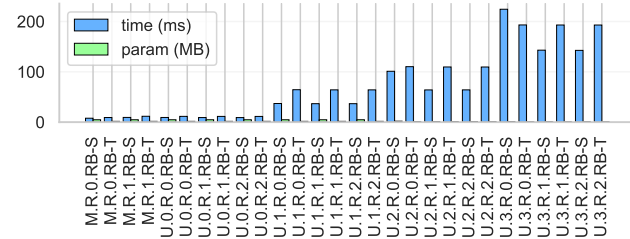


Figure A2: Time and Parameters of the blocks in the VAE decoder.

Reconstruction Results of the Compressed VAE Decoder. The VAE decoder in the I2V task consumes a significant amount of inference time. To address this, we further compress the VAE decoder in the VDMini-I2V model. We employ layer pruning and channel pruning techniques to accelerate the VAE decoder, followed by fine-tuning on the OpenVid-1M dataset using reconstruction loss, perceptual loss, and adversarial loss as described in [17]. As shown in Table A1, the inference time of the compressed VAE decoder is reduced by 70%, and the model has 30% fewer parameters compared to the original. As provided in Table A2, we report the PSNR, SSIM, and LPIPS on the UCF101 dataset, and the reconstruction results are illustrated in Figure A3.

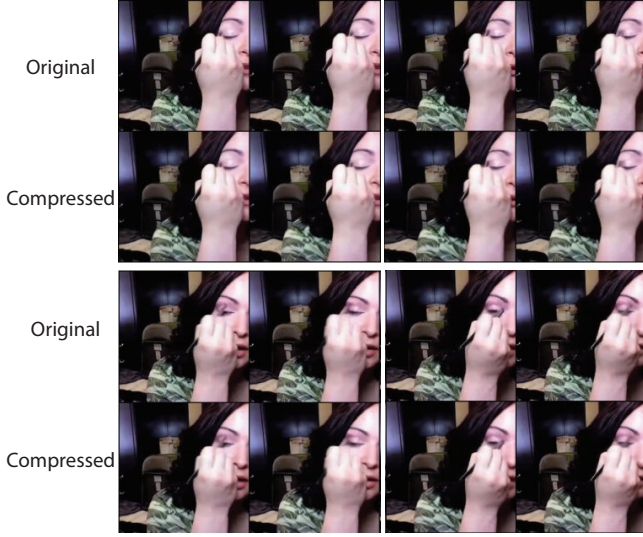


Figure A3: Reconstruction results of the VAE decoder. The compressed VAE decoder achieves image quality metrics comparable to the original VAE decoder while being significantly faster. For instance, decoding a video latent of size $14 \times 72 \times 128$ takes 2832ms with the original VAE decoder, compared to only 840.5ms with the compressed VAE decoder.

Table A1: Comparison of the model architecture and inference latency between SF-V and our proposed VDMini-I2V.

Model	CLIP Encoder	VAE Encoder	U-Net	VAE Decoder
	224 × 224	576 × 1024	14 × 72 × 128	14 × 72 × 128
SF-V	#Param (M)	632.08	34.16	1524.62
	Latency (ms)	35	75	512
VDMini-I2V	#Param (M)	632.08	34.16	940.9
	Latency (ms)	35	75	345
				840.5

Table A2: Quantitative comparison of the image quality metrics on the UCF101 dataset between the original VAE decoder and the compressed VAE decoder.

VAE Decoder	PSNR \uparrow	SSIM \uparrow	LPIPS \downarrow
Original	32.30	0.94	0.031
Compressed	31.41	0.93	0.039

Table A3: Comparison of the model architecture and inference latency between T2V-Turbo-v2 and our proposed VDMini-T2V.

Model	Text Encoder	U-Net	VAE Decoder	
	Resolution	77 Tokens	16 × 40 × 64	
T2V-Turbo-v2	Inference Steps	1	16	1
	#Param (M)	354.03	1413.65	49.49
VDMini-T2V-Turbo	Latency (ms)	13.57	2554.05	367.66
	#Param (M)	354.03	817.02	49.49
	Latency (ms)	13.57	1662.26	367.66

B DETAILS ABOUT THE COMPRESSED U-NET

Most I2V and T2V models share nearly identical architectures in their diffusion model backbone (*i.e.*, U-Net). For instance, classical VDMs such as VideoCrafter [8] and Open-Sora [74] utilize the exact same U-Net architecture for both I2V and T2V tasks. Consequently, it is reasonable to assume that specific blocks within these U-Nets perform similar roles across both tasks. Hence, in this work, we focus on providing an in-depth analysis of the I2V model SF-V and extend our observations to the T2V model T2V-Turbo-v2.

Specifically, we study the **importance score** and the **computational complexity** for the U-Net of SF-V. First, we present the detailed block-wise importance scores by replacing the blocks with identity mapping or a single convolutional layer, as shown in Figure A4. A higher FVD score indicates a more important block. The FVD score calculation follows the evaluation protocol introduced in StyleGAN-V [56]. For fast evaluation, we sample 1200 videos from the UCF101 dataset as the ground-truth videos and calculate the FVD score between the generated and ground-truth videos. As illustrated in Figure A4, we use a specific notation to denote the blocks in the U-Net. For example, the module named “D.1.R.0.RB-S” indicates: “D” for DownBlock, “1” for the first subblock, “R” for ResBlock type, “0” for the layer index of the ResBlock, and “RB-S” for SpatialResBlock consisting of 2D ResNet blocks. The results show that the SpatialResBlock in the DownBlocks is more important than other sub-blocks, and in the UpBlocks, the SpatialAttentionBlock is more important. Second, we present the computational complexity study, including the inference time and the number of parameters for each block in the U-Net of SF-V, as shown in Figure A5. The inference time measurement is conducted on a single NVIDIA A100 GPU. Additionally, we present the first and last frames of the videos generated by the pruned model in Figure A6. When removing D.2 or U.1, the generated videos exhibit subtle motion.

According to the above observations, we propose the following pruning strategy for VDMini. 1) completely remove the “Down-3”, “Mid”, and “Up-0” blocks in VDMini, and 2) reduce the number of blocks in “Down-0”, “Down-1”, “Up-2”, and “Up-3” by one compared to the original U-Net.

As explained previously, we directly apply our observations regarding U-Net compression from the I2V model to the T2V model. Consequently, as shown in Table A4, the pruned models VDMini-T2V and VDMini-I2V share an almost identical architecture, with only minor differences in the structure of the “ResBlock.” Specifically, in VDMini-T2V, the ResBlock is a 2D ResNet block, while in VDMini-I2V, it consists of both a 2D ResBlock and a 3D ResBlock.

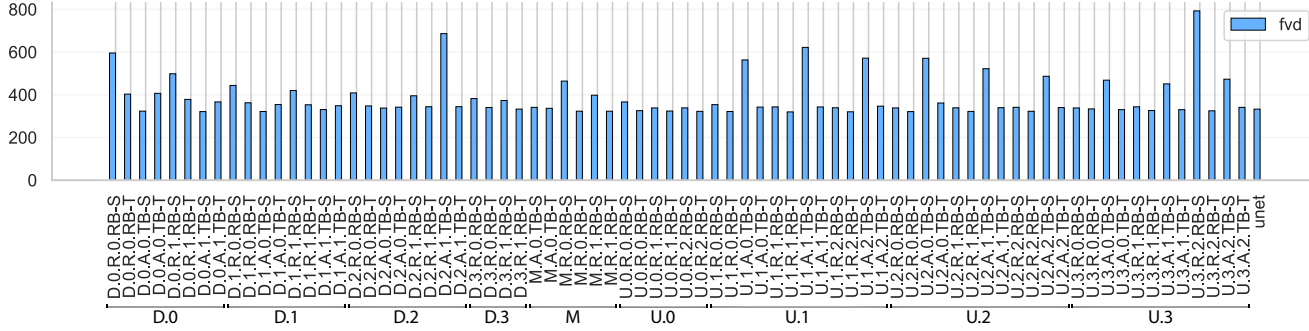


Figure A4: Block-wise FVD score by removing or replacing the blocks in the U-Net.

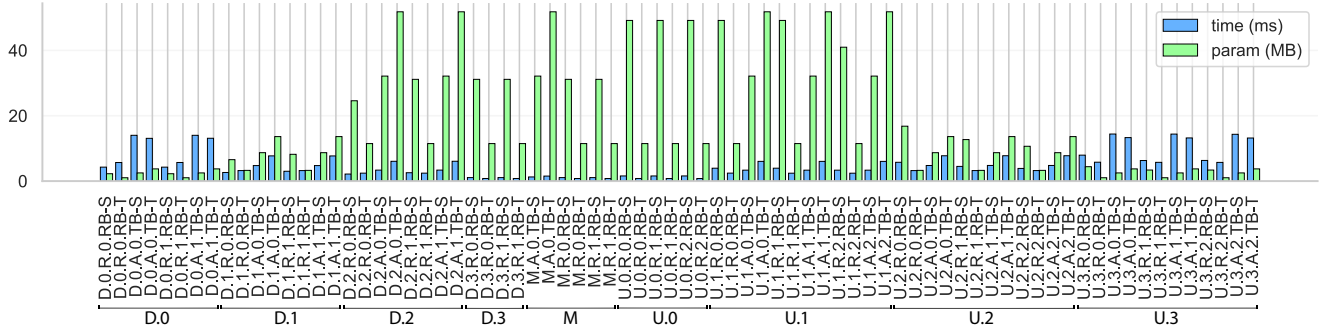


Figure A5: Block-wise inference time and parameter count in the U-Net.

Table A4: The detailed architecture of the compressed U-Net used in VDMINI.

Stage	Resolution	Type	Config	UNet Model	
				Origin	Ours
Down-0	$T \times \frac{H}{8} \times \frac{W}{8}$	ResBlock	Dimension # Blocks	320 2	320 1
		TransformerBlock	Dimension # Blocks	320 2	320 1
Down-1	$T \times \frac{H}{16} \times \frac{W}{16}$	ResBlock	Dimension # Blocks	640 2	640 1
		TransformerBlock	Dimension # Blocks	640 2	640 1
Down-2	$T \times \frac{H}{32} \times \frac{W}{32}$	ResBlock	Dimension # Blocks	1280 2	1280 2
		TransformerBlock	Dimension # Blocks	1280 2	1280 2
Down-3	$T \times \frac{H}{64} \times \frac{W}{64}$	ResBlock	Dimension # Blocks	1280 2	1280 0
Mid	$T \times \frac{H}{64} \times \frac{W}{64}$	ResBlock	Dimension # Blocks	1280 2	1280 0
		TransformerBlock	Dimension # Blocks	1280 1	1280 0
Up-0	$T \times \frac{H}{64} \times \frac{W}{64}$	ResBlock	Dimension # Blocks	1280 3	1280 0
Up-1	$T \times \frac{H}{32} \times \frac{W}{32}$	ResBlock	Dimension # Blocks	1280 3	1280 3
		TransformerBlock	Dimension # Blocks	1280 3	1280 3
Up-2	$T \times \frac{H}{16} \times \frac{W}{16}$	ResBlock	Dimension # Blocks	640 3	640 2
		TransformerBlock	Dimension # Blocks	640 3	640 2
Up-3	$T \times \frac{H}{8} \times \frac{W}{8}$	ResBlock	Dimension # Blocks	320 3	320 2
		TransformerBlock	Dimension # Blocks	320 3	320 2



Figure A6: Visual analysis of the pruned SF-V.

C IMPLEMENTATION OF I2V AND T2V BASELINES

Here, we introduce the implementation details of our I2V and T2V baseline methods SF-V and T2V-Turbo-v2.

SF-V.: [72] is a one-step I2V model fine-tuned from Stable Video Diffusion (SVD) [3] on a 1M internal video dataset. SF-V follows LADD [55] to fine-tune the pre-trained SVD with adversarial loss, with the discriminator initialized from the pre-trained SVD. Since the code and model of SVD are not publicly available, we re-implemented the SF-V model using the OpenVid-1M dataset, a high-quality video dataset with dense captions. We adhered to the original SF-V training settings, with a batch size of 32 and a gradient accumulation step of 4. The learning rates for the U-Net and the heads of the

Table A5: Evaluation of Hunyuan model on VBench-T2V.

Models	Quality Score ↓	Semantic Score ↓	Total Score ↓	#Double-Stream Layer	#Single-Stream Layer	Inference Speed(ms)
HunyuanVideo	85.09%	75.82%	83.24%	20	40	366.11
VDMini-T2V-HY	84.34%	74.76%	82.42%	12	28	292.89

discriminator were set to 1e-5 and 1e-4, respectively. After 50K training steps, we achieved an FVD score of 166.26, comparable to the original SF-V model.

T2V-Turbo-v2. [39] is a T2V model, which is distilled from VideoCr after2 [9] and follows a consistency distillation scheme. The initial version of T2V-Turbo (*i.e.*, T2V-Turbo-v1) adopts mixed reward models to enhance the generation quality and prompt consistency, and T2V-Turbo-v2 further employs MotionClone [42] to enhance the motion dynamics in the few-step sampling, and the resulting model achieves the first rank in the VBench leaderboard. The U-Net architecture of T2V-Turbo-v2 is similar to SVD.

HunyuanVideo. is a large-scale T2V model with cutting-edge performance. HunyuanVideo is based on the Diffusion Transformer (DiT) architecture, which is with size of 13B parameters in total. The model is consisted of multiple components: CLIP and MLLM for text encoding, a 3D VAE for image/video encoding and decoding, and a DiT for video latent generation. Inspired by SD3 [16] Hunyuan-Video is trained with a curated dataset with vase image/video-text

pairs, the training framework follows the flow matching. The released model could achieve competitive generation quality with the state-of-the-art commercial models such as Luma and Gen-3.

D IMPLEMENTATION DETAILS FOR VDMINI-T2V-HY

We acknowledge that the issues of subtle motion and short duration are inherent limitations of the base models. Therefore, we conduct extensive experiments on the DiT-based model HunyuanVideo [35], the results are reported in Table A5.

For training the VDMini-T2V model based on HunyuanVideo, we follow the full fine-tuning strategy introduced in FastVideo, which includes velocity prediction loss introduced in flow matching and our proposed ICMD loss. The learning rate for DiT and the discriminator are set to 5e-6 and 1e-5, respectively. The batch size is set to 8 for fine-tuning with 30K steps. The loss weight for ICD and MCA loss are same as VDMini-T2V based on T2V-Turbo-v2.